

A NUMERICAL IMPLEMENTATION OF FOKAS BOUNDARY INTEGRAL APPROACH: LAPLACE'S EQUATION ON A POLYGONAL DOMAIN

BENGT FORNBERG* AND NATASHA FLYER†

Abstract. A recently discovered transform approach allows a large class of initial and initial-boundary value problems to be solved in terms of contour integrals. We introduce here a spectrally accurate numerical discretization of this approach for the case of Laplace's equation on a polygonal domain, and compare it against an also spectrally accurate implementation of the traditional boundary integral formulation.

Key words. Boundary integral method, global equations, Dirichlet-Neumann map, Laplace equation, Fokas transform method, polygonal domain.

1. Introduction. About a decade ago, Fokas and collaborators introduced a new analytic transform technique which provides closed form solutions (in terms of contour integrals) for a variety of PDE boundary value (BV) and initial-boundary value (IBV) problems [6, 7, 8, 9]. For several dispersive IBV problems, numerical implementations of these integrals have been found to offer opportunities that in some respects improve on previously available techniques [4, 10, 11]. In the case of the Dirichlet-Neumann map problem for elliptic equations, the Fokas approach provides a direct alternative to regular boundary integral (BI) methods in the sense that it also requires discretization only along the domain boundary, and not throughout the interior of the domain. The new formulation provides a spectral (Fourier) space analogue of the usual BI method, which is formulated in the physical space.

This present study will focus on simple polygonal domains and, in particular, on the trapezoidal domain displayed in Figure 1.1. We introduce here a spectrally accurate implementation (assuming the solutions themselves are sufficiently smooth), i.e. the relevant errors decrease as $O(e^{-cN})$ where N is the number of parameters used for discretization along each side, and $c > 0$ is some constant. Thus, low values for N often suffice for high accuracy. We recall that most previous numerical implementations of this new analytic formulation have been limited to a relatively low $O(N^{-2})$ algebraic rate of convergence [10, 11, 12]. However, the possibility of spectral convergence (by discretizing with Chebyshev rather than Fourier expansions along the boundaries) was noted in [18].

The goals of the present study are to show that (i) Legendre expansions allow key integrals to be evaluated in closed form, (ii) no iterative linear algebra algorithms are needed, and (iii) corner singularity corrections can be successfully incorporated in the procedure. Brief numerical comparisons are provided between the new and the traditional BI methods, and also with a direct collocation method based on sets of Laplace solutions.

We recall that traditional BI implementations (as surveyed in [16]), often encounter difficulties with certain quadrature evaluations. As a result, it is common to discretize the boundary into a large number of *boundary elements*, generally leading to low order algebraic convergence rates. We use here for our comparisons an implementation of the traditional BI formulation which also features spectral accuracy.

*University of Colorado, Department of Applied Mathematics, 526 UCB, Boulder, CO 80309, USA (fornberg@colorado.edu).

†National Center for Atmospheric Research, Boulder, CO 80305, USA (flyer@ucar.edu).

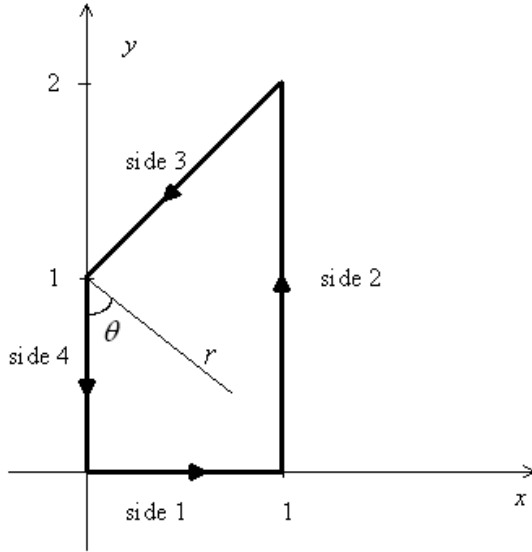


FIG. 1.1. Domain in the (x,y) -plane for our test problems, together with key notation.

It should be noted that conformal mapping based methods can be very effective for the Laplace equation on polygonal domains [1]. However, we do not consider this approach since, in contrast to BI methods, it cannot be generalized to other types of PDEs.

2. Governing equation and three analytical formulations. We consider Laplace's equation

$$\Delta q \equiv \frac{\partial^2 q}{\partial x^2} + \frac{\partial^2 q}{\partial y^2} = 0 \quad (2.1)$$

over the bounded 2-D domain Ω shown in Figure 1.1. Either $q(x,y)$ or $q_n(x,y)$ (normal derivative in the outward direction) is specified along each section of the domain boundary $\partial\Omega$. This paper focuses on the Dirichlet-Neumann map problem, which amounts to finding, along each section, the condition that was not specified. We next describe three different analytical formulations which all lead to practical numerical algorithms. None of them will require any discretization within Ω to solve the problem.

2.1. New BI (BI-F) formulation. The first analytical formulation we consider is based on the works of Fokas cited above. The Dirichlet-Neumann map is described by the following pair of integral relations that must hold when integrating around the domain boundary

$$\oint_{\partial\Omega} e^{-i k z} \left(k \frac{dz}{ds} q(s) + q_n(s) \right) ds = 0, \quad (2.2)$$

$$\oint_{\partial\Omega} e^{i k \bar{z}} \left(k \frac{d\bar{z}}{ds} q(s) - q_n(s) \right) ds = 0. \quad (2.3)$$

The integrals are taken in the positive direction, and s is the arc length. The complex variable $z = x + i y$ denotes locations in the (x,y) -plane. Complex conjugation is

defined in the usual way, i.e. $\bar{z} = x - i y$. The equations (2.2), (2.3) are called the *global relations*. They hold for any value of the complex variable k . By choosing different values for k , they provide an unlimited number of independent relations between $q(s)$ and $q_n(s)$.

We are in this study not concerned with calculating $q(x, y)$ at locations in the domain interior. This can however be achieved by evaluating a succession of integrals, as described in [10], equations (11.3)-(11.5).

2.2. Traditional BI (BI-T) formulation. The second analytical formulation we consider is the traditional BI method. In this case, the key relation linking $q(\underline{\xi})$ and $q_n(\underline{\xi})$ around the boundary is

$$\frac{1}{2}q(\underline{x})\Big|_{\underline{x}\in\partial\Omega} = -\oint_{\partial\Omega} (G_n(\underline{x}, \underline{\xi}) q(\underline{\xi}) + G(\underline{x}, \underline{\xi}) q_n(\underline{\xi})) ds, \quad (2.4)$$

where

$$G(\underline{x}, \underline{\xi}) = \frac{1}{2\pi} \log |\underline{x} - \underline{\xi}| \quad (2.5)$$

is the infinite domain Green's function and $G_n(\underline{x}, \underline{\xi})$ is its outward pointing normal derivative. This function $G(\underline{x}, \underline{\xi})$ satisfies (2.1) for $\underline{x} \neq \underline{\xi}$ where \underline{x} is an abbreviated notation for (x, y) . The variable s represents again the arc length, and $\underline{\xi} = \underline{\xi}(s)$ traces out the boundary $\partial\Omega$. Since \underline{x} can be any point along the boundary $\partial\Omega$, we again obtain an unlimited number of independent relations between $q(\underline{\xi})$ and $q_n(\underline{\xi})$.

If, in addition to solving the Dirichlet-Neumann problem, one wants to obtain the solution $q(\underline{x})$ throughout the inside of Ω , this can in the BI-T formulation be achieved very simply by replacing $\frac{1}{2}q(\underline{x})\Big|_{\underline{x}\in\partial\Omega}$ with $q(\underline{x})\Big|_{\underline{x}\in\Omega}$ in (2.4), i.e.

$$q(\underline{x})\Big|_{\underline{x}\in\Omega} = -\oint_{\partial\Omega} (G_n(\underline{x}, \underline{\xi}) q(\underline{\xi}) + G(\underline{x}, \underline{\xi}) q_n(\underline{\xi})) ds. \quad (2.6)$$

The difference by a factor of two stems from the fact that (2.4), with $\underline{x} \in \partial\Omega$, should be interpreted as a principle value integral. It therefore picks up only half of the contribution from the singularity in $G_n(\underline{x}, \underline{\xi}) q(\underline{\xi})$ at the location $\underline{\xi} = \underline{x}$ compared to the case when \underline{x} is inside Ω .

If one adheres to the (unusual) convention of assigning the value of a principal value integral to the limit when reaching the boundary from the inside, the relation (2.6) can then, for our 4-sided polygonal domain, be written very conveniently as

$$\sum_{\nu=1}^4 \left(\int_{\text{side } \nu} (\delta_\nu G_n(\underline{x}, \underline{\xi}) q^{(\nu)}(\underline{\xi}) + G(\underline{x}, \underline{\xi}) q_n^{(\nu)}(\underline{\xi})) ds \right) = 0 \quad (2.7)$$

where

$$\delta_\nu = \begin{cases} -1 & \text{if } \underline{x} \text{ is located on side } \nu \\ +1 & \text{if } \underline{x} \text{ is located on a side different from } \nu \end{cases} .$$

2.3. Collocation with sets of Laplace solutions (CLS). It is straightforward to find infinite sets of solutions to Laplace's equation. The CLS approach amounts to combining such solutions, so that the specified boundary conditions also

become satisfied. Examples of Laplace solutions include the real and/or the imaginary parts of any set of analytic functions, such as z^μ or $e^{i\mu z}$, μ integer. It is often advantageous to consider solution sets that include functions with certain corner properties. The survey article [15] discusses both the analytic form of corner singularities for Laplace's equation, and some numerical approaches for handling them. With regard to our specific test domain (using the notation in Figure 1.1), we note that the functions

$$g_\mu(r, \theta) = r^{\frac{2}{3}(2\mu-1)} \sin\left(\frac{2}{3}(2\mu-1)\theta\right), \quad \mu = \text{integer} \quad (2.8)$$

satisfy Laplace's equation

$$\Delta g \equiv \frac{1}{r} \frac{\partial}{\partial r} \left(r \frac{\partial g}{\partial r} \right) + \frac{1}{r^2} \frac{\partial^2 g}{\partial \theta^2} = 0$$

for $r > 0$ as well as the boundary conditions

$$\text{Side 3: } \frac{\partial}{\partial \theta} g_\mu(r, \theta)|_{\theta=3\pi/4} = 0, \quad (2.9)$$

$$\text{Side 4: } g_\mu(r, \theta)|_{\theta=0} = 0.$$

Hence, the same will hold for all linear combinations of these functions

$$q(r, \theta) = \sum_{\mu=1}^{\infty} c_\mu g_\mu(r, \theta). \quad (2.10)$$

Assuming we are only interested in bounded solutions, we include in the sum only terms with $\mu \geq 1$. The functions in this sum are known as stress (or flux) intensity factors, with the coefficient for the $\mu = 1$ function $g_1(r, \theta) = r^{\frac{2}{3}} \sin(\frac{2}{3}\theta)$ often of particular interest.

For the remaining three corners (with interior angles 45° and 90°), singularities will arise only if the BCs are inconsistent with the PDE (a situation encountered in Test Problem 3) or are inconsistent with differentiated versions of the PDE. For example, the expressions

$$\begin{aligned} h_\mu(r, \theta) &= \frac{(-1)^\mu 2r^{2\mu}}{\pi} (\theta \cos 2\mu\theta + \log r \sin 2\mu\theta) \\ &= \frac{(-1)^\mu}{\pi} \text{Im}(z^{2\mu} \log z) \quad , \quad \mu = 1, 2, \dots \end{aligned} \quad (2.11)$$

satisfy Laplace's equation $\Delta h_\mu = 0$ for $r > 0$ together with $h_\mu(r, 0) = 0$ and $h_\mu(r, \frac{\pi}{2}) = r^{2\mu}$, i.e. they violate $\Delta^\mu h_\mu \equiv \left(\frac{\partial^2}{\partial x^2} + \frac{\partial^2}{\partial y^2} \right)^\mu h_\mu = 0$, $\mu > 1$, at $r = 0$. When such violations occur, there exists logarithmic singularities at the corner, as indicated by (2.11). In the worst locally bounded case ($\mu = 1$), this type of singularity will be of the form $r^2 \log r$, i.e. much milder than the singularities that are typical for when sides with Dirichlet and Neumann conditions meet at a 135° corner. We recall that corner singularities can also arise for IBV problems, often with more complex singularity structures [5].

3. Numerical implementation strategies.

3.1. BI-F formulation. If the unknown parts of $q(s)$ and $q_n(s)$ in (2.2) and (2.3) are discretized by N parameters along each of the four sides, we need to use $K \geq 2N$ different complex values for k , in order to get a sufficient number of equations for the unknowns parameters. Utilizing Legendre expansions for these discretizations leads to spectral accuracy and also to key integrals of a form that can be evaluated analytically. The first step in this process is to parameterize each side of the domain using a new variable $t \in [-1, 1]$. The equations (2.2), (2.3) then become

$$\sum_{\text{all sides}} \left(\int_{-1}^1 e^{-i k z} \left(k \frac{dz}{dt} q(t) + \frac{ds}{dt} q_n(t) \right) dt \right) = 0 \quad (3.1)$$

$$\sum_{\text{all sides}} \left(\int_{-1}^1 e^{i k \bar{z}} \left(k \frac{d\bar{z}}{dt} q(t) + \frac{ds}{dt} q_n(t) \right) dt \right) = 0 \quad (3.2)$$

For the present domain geometry, we obtain

$$\begin{array}{lll} \text{Side 1:} & z = \frac{1}{2}(t+1) & \frac{dz}{dt} = \frac{1}{2} & \frac{ds}{dt} = \frac{1}{2} \\ \text{Side 2:} & z = 1 + i(t+1) & \frac{dz}{dt} = i & \frac{ds}{dt} = 1 \\ \text{Side 3:} & z = 1 + 2i - \frac{1}{2}(t+1)(1+i) & \frac{dz}{dt} = -\frac{1}{2}(1+i) & \frac{ds}{dt} = \frac{1}{\sqrt{2}} \\ \text{Side 4:} & z = i - \frac{i}{2}(t+1) & \frac{dz}{dt} = -\frac{i}{2} & \frac{ds}{dt} = \frac{1}{2} \end{array} \quad (3.3)$$

For each of these k -values, chosen as discussed in Appendix A, we evaluate (analytically if possible, else numerically by adaptive Gaussian quadrature), the integrals in (3.1) and (3.2) for which either q or q_n have been specified. The unknown function along each of the four sides $\nu = 1, \dots, 4$ will be represented as Legendre expansions with unknown coefficients

$$\sum_{m=0}^{N-1} c_m^{(\nu)} P_m(t). \quad (3.4)$$

Substituting (3.4) into (3.1) and (3.2) leads to integrals of the general form

$$\int_{-1}^1 e^{\alpha t} P_m(t) dt = \frac{2^{m+1} \alpha^m m!}{(2m+1)!} {}_0F_1\left(m + \frac{3}{2}, \left(\frac{\alpha}{2}\right)^2\right) = \frac{\sqrt{2\pi\alpha}}{\alpha} I_{m+\frac{1}{2}}(\alpha). \quad (3.5)$$

Here, α is the coefficient that appears in front of the t -term in the exponent $-ikz$ in case of (3.1) and $ik\bar{z}$ in case of (3.2) when using the appropriate formula for z (dependent on the side number according to the leftmost column in (3.3)). The integral stated in (3.5) is an entire function of α . We have written the factor in front of the Bessel I function as $\frac{\sqrt{2\pi\alpha}}{\alpha}$ instead of $\sqrt{\frac{2\pi}{\alpha}}$, in order for the branch cuts along the negative real axis for the square root and for the Bessel I function to cancel out when using the standard branch cut conventions for these two functions.

Each of the four domain sides contains N unknowns ($c_m^{(\nu)}$, $m = 0, 1, \dots, N-1$). Hence (3.1) and (3.2) take the form of $2K$ linear equations for these $4N$ expansion coefficients $c_m^{(\nu)}$. As noted above, one needs to choose $K \geq 2N$. Numerical tests show that larger values of K generally gives more robust and accurate results, with $K = 5N$ a good routine choice. The general structure of the overdetermined linear system is illustrated in Figure 3.1. A standard linear systems solver (such as the “\”-operator in Matlab) provides the unknown expansion coefficients. The corresponding boundary functions then follow from (3.4).

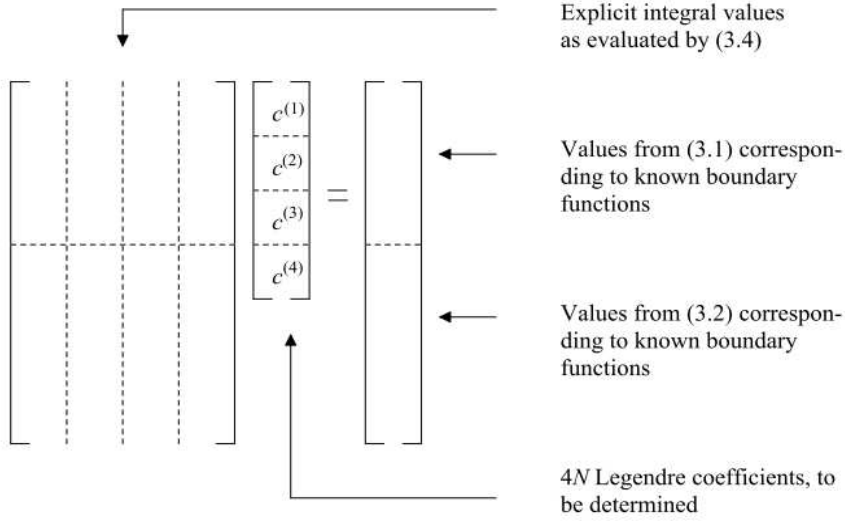


FIG. 3.1. Structure of the linear system that arises in the BI-F method.

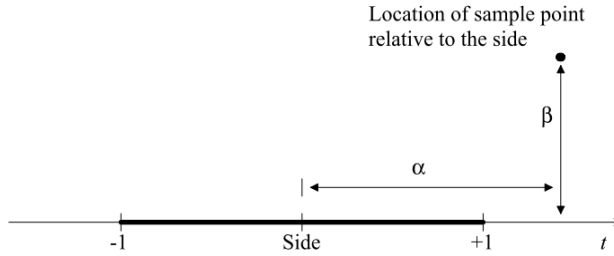


FIG. 3.2. Illustration of the parameters α and β appearing in (3.6) and (3.7).

3.2. BI-T formulation. The relation (2.7) will hold for every value \underline{x} that we choose on $\partial\Omega$. As a first step, we again change the parameterization separately for each side, from arc length s to $s = s(t)$ with $t \in [-1, 1]$. Relative to this interval in a t -plane, the sample point $\underline{x} = (x, y)$ will be at some location (α, β) - illustrated in Figure 3.2 for the case that the sample point is located on a different side than the one we just now are integrating along. Along the t -axis, (2.5) will take the form

$$G(t) = c \log[(\alpha - t)^2 + \beta^2]$$

where c is some constant that follows from the variable change that brought the side to $t \in [-1, 1]$. Then

$$G_n(t) = -2c \frac{\beta}{(\alpha - t)^2 + \beta^2}.$$

Hence, the integrals that arise from (2.7) will become of the general forms

$$\int_{-1}^1 f(t) \log \sqrt{(\alpha - t)^2 + \beta^2} dt, \quad (3.6)$$

and

$$\int_{-1}^1 f(t) \frac{\beta}{(\alpha - t)^2 + \beta^2} dt, \quad (3.7)$$

respectively, where $f(t)$ will either be known or unknown functions. If \underline{x} is actually located on the side that here is parameterized by $t \in [-1, 1]$, β becomes zero and the second integral (3.7) will need to be interpreted as a principal value integral. Most standard numerical quadrature methods face difficulties both for $\beta = 0$ (when (3.6) features a log-type singularity at $t = \alpha$), and for small non-zero values of β .

Legendre expansions are again well suited for discretization of the q and the q_n -functions along sides $\nu = 1, \dots, 4$:

$$q^{(\nu)}(t) = \sum_{m=0}^{N-1} c_m^{(\nu)} P_m(t), \quad (3.8)$$

$$q_n^{(\nu)}(t) = \sum_{m=0}^{N-1} d_m^{(\nu)} P_m(t). \quad (3.9)$$

Substituting such expansions for $f(t)$ in (3.6) and (3.7) leads thus to integrals of the general type

$$A_m(\alpha, \beta) = \int_{-1}^1 P_m(t) \log \sqrt{(\alpha - t)^2 + \beta^2} dt, \quad (3.10)$$

$$B_m(\alpha, \beta) = \int_{-1}^1 P_m(t) \frac{\beta}{(\alpha - t)^2 + \beta^2} dt. \quad (3.11)$$

Just as with the Legendre integrals (3.5) arising in the context of the BI-F formulation, integrals of the general forms (3.10), (3.11) can be quickly evaluated in closed form, as shown in Appendix B. The algorithm for $B_m(\alpha, \beta)$ is designed so that the value $B_m(\alpha, 0)$ coincides with the limit value for $\beta \searrow 0$. In our context, the algorithm therefore provides the convenience of making (2.7) valid also when $\underline{x} \in \partial\Omega$.

Substituting (3.8) and (3.9) into (2.7) and carrying out the changes of variables outlined above gives, for every \underline{x} -value that we choose on the boundary $\partial\Omega$, a linear relation between all the $c_m^{(\nu)}$ and $d_m^{(\nu)}$ entries, of the general form

$$\sum_{\nu=1}^4 \left(\sum_{m=0}^{N-1} \sigma_{m,\nu} c_m^{(\nu)} + \tau_{m,\nu} d_m^{(\nu)} \right) = 0. \quad (3.12)$$

Here all the $8N$ entries $\sigma_{m,\nu}$ and $\tau_{m,\nu}$ ($m = 0, 1, \dots, N-1$, $\nu = 1, \dots, 4$) are explicitly known numbers (obtained by evaluating the integrals $A_m(\alpha, \beta)$ and $B_m(\alpha, \beta)$ described in (3.10) and (3.11)). Figure 3.3 illustrates the ‘structure’ of these $4N$ relations (3.12) (one relation for each of the $4N$ sample points along $\partial\Omega$) when they are written out in matrix/vector form. Having arrived at this linear algebra relationship, the numerical solution procedure proceeds as follows: Along each side on which either $q^{(\nu)}(t)$ or $q_n^{(\nu)}(t)$ is given, use (3.8) or (3.9) to compute the known entries in the long column vector shown in Figure 3.3. After these are multiplied with their respective columns in the coefficient matrix and moved to the system’s right hand side, we are left with a square linear system for the unknown Legendre expansion coefficients.

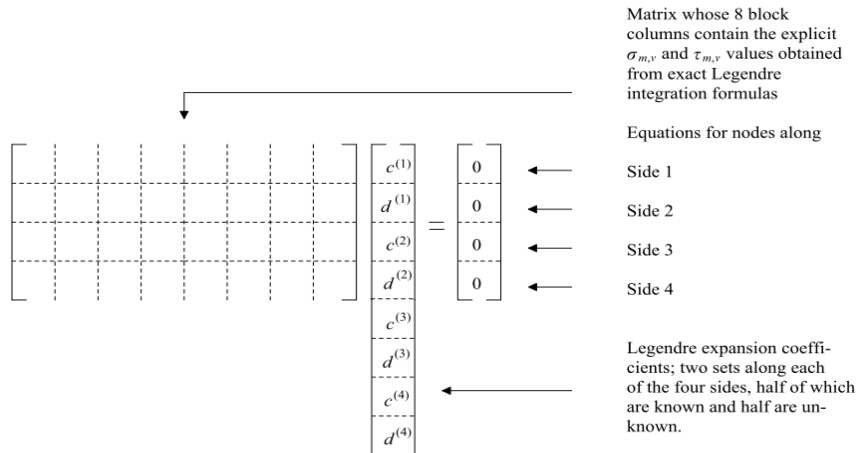


FIG. 3.3. Structure of the linear system that arises in the BI-T method.

With the present numerical method, tests showed that there were no benefits to be gained by using a larger number of sample points than unknown coefficients. Tests also showed that a good strategy is to select the sample points \underline{x} along each of the four sides as the zeros of the degree N Chebyshev polynomial. This clusters nodes towards the ends of each side, but avoids evaluations exactly at the corners.

3.3. CLS formulation. We will not attempt here to present a systematic discussion of how to best use this approach for general Dirichlet-Neumann problems. Our present ad hoc implementation of choosing some set of Laplace solutions and then forcing their combination to satisfy all the boundary conditions, requires only a few lines of code and can yield excellent results. A different CLS version (enforcing the boundary conditions weakly via Lagrange multipliers) was introduced in [14] and later used in [2]. For our implementation, in the last two test problems of this paper, the function set we use already satisfies the boundary conditions along two of the four sides, and it only remains to collocate along the remaining two sides. We do this by selecting N nodes along these two sides (again distributed as the Chebyshev zeros), and then impose that the function set (2.10), truncated to $2N$ terms, obeys the boundary data at these points. The structure of the resulting linear system is seen in Figure 3.4.

4. Statements of the three test cases. We will consider three different choices of boundary conditions for the domain in Figure 1.1:

Test Case 1 (no singularity): This test case is chosen so that the provided boundary data will be satisfied by

$$q(x, y) = e^{1+x} \cos(2 + y). \quad (4.1)$$

The above function is the real part of the entire function e^{z+1+2i} . We specify q along the Sides 1, 2, 4 and q_n along Side 3 (all according to (4.1)), and the task is to compute the unknown boundary values along each of the four sides, i.e. q along Side 3 and q_n along Sides 1, 2, 4.

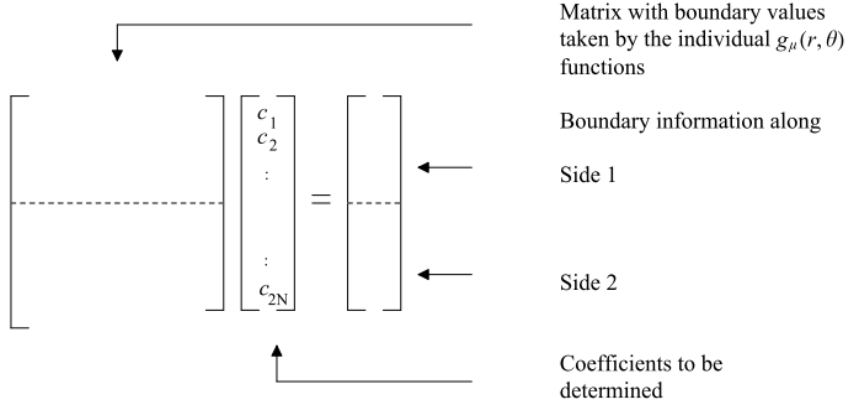


FIG. 3.4. Structure of the linear system that arises in the CLS method in case of Test Problems 2 and 3.

Test Case 2 (one corner singularity): Following [3] and [13], we specify:

$$\begin{aligned} \text{Side 1: } q_n &= 0, & \text{Side 2: } q &= 1, \\ \text{Side 3: } q_n &= 0, & \text{Side 4: } q &= 0. \end{aligned}$$

This problem features one singular point located at the 135° corner $(x, y) = (0, 1)$.

Test Case 3 (all corners singular): This case is taken from [2]. A reformulation of equation (4) in [2] in terms of $q(x, y)$ along Sides 1 and 2 gives the following boundary conditions

$$\begin{aligned} \text{Side 1: } q &= \frac{1}{6\pi} (3\pi x^2 + 2(1 - x^2) \arctan(x) + 2x \log(1 + x^2)) \\ \text{Side 2: } q &= \frac{1}{6\pi} \left(3\pi + 2y(y - 2) \arccos\left(\frac{1-y}{\sqrt{y^2 - 2y + 2}}\right) - 2(y - 1) \log(y^2 - 2y + 2) \right) \\ \text{Side 3: } q_n &= 0 \\ \text{Side 4: } q &= 0 \end{aligned}$$

In this case, there are singularities at all four corners. The strongest singularity is located at $(0, 1)$, and is locally of the type given by (2.8).

5. Numerical results for the three test cases.

5.1. Test Case 1. In terms of the variable t , the values for $q(t)$ and $q_n(t)$ along the four sides follow directly from (4.1)

$$\begin{aligned} \text{Side 1: } q &= e^{(3+t)} \cos(2) & q_n &= e^{(3+t)} \cos(2) \\ \text{Side 2: } q &= e^2 \cos(3 + t) & q_n &= e^2 \cos(3 + t) \\ \text{Side 3: } q &= e^{(3-t)/2} \cos\left(\frac{7-t}{2}\right) & q_n &= \frac{1}{\sqrt{2}} e^{(3-t)/2} (\cos\left(\frac{7-t}{2}\right) + \sin\left(\frac{7-t}{2}\right)) \cdot \\ \text{Side 4: } q &= e \cos\left(\frac{5-t}{2}\right) & q_n &= e \cos\left(\frac{5-t}{2}\right) \end{aligned} \quad (5.1)$$

Since we have the exact answer available, it is straightforward to calculate the largest absolute error in any of the four unknown functions. This yields the result displayed in Figure 5.1. Several observations can be made:

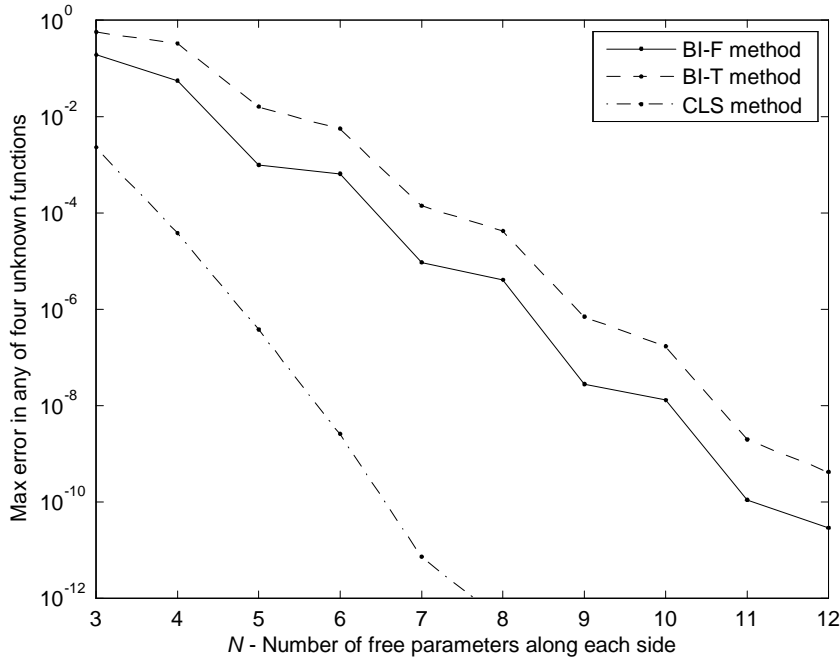


FIG. 5.1. *Test Case 1: Maximum error in any of the unknown boundary functions plotted vs. N - the number of free parameters used in the discretization along each side. The linear trends in this log-linear display indicates spectral convergence.*

- The BI-F method requires the selection of the parameter R - the radius of the circle within which the k -values are to be taken. Numerical experimentation suggest that the choice of R is not critical and, in the present test, values within the range $8 \leq R \leq 20$ generally worked well. A good general strategy is to choose R so as to keep the system condition number low.
- For the CLS method, we used as basis functions $\{1, \{\text{Re}(z^k), \text{Im}(z^k), k = 1, 2, \dots\}\}$, i.e. $\{1, x, y, x^2 - y^2, 2xy, \dots\}$.
- The excellent performance of the CLS approach seen in Figure 5.1 is somewhat misleading, as the solution to the present test problem is the real part of an entire function. Typical Laplace solutions will feature singularities in domain corners or, at the very least, in the near vicinity of the domain, ruining spectral convergence of this approach (or convergence altogether), unless care has been taken in finding a specially designed set of expansion functions. The other two methods (BI-F and BI-T) do not assume continuity at corners or any regularity when solutions are continued to outside the domain. This makes the BI approaches applicable to more general situations.
- If the condition number for a linear system approaches 10^{16} , there is a serious danger that rounding errors have compromised many of the digits (when using standard 16 digit arithmetic precision). Although not an ideal measure of numerical sensitivity (especially when very high), the low condition numbers seen for both of the BI implementations in Figure 5.2 indicate good robustness for these methods against numerical 'noise' (due to either machine rounding

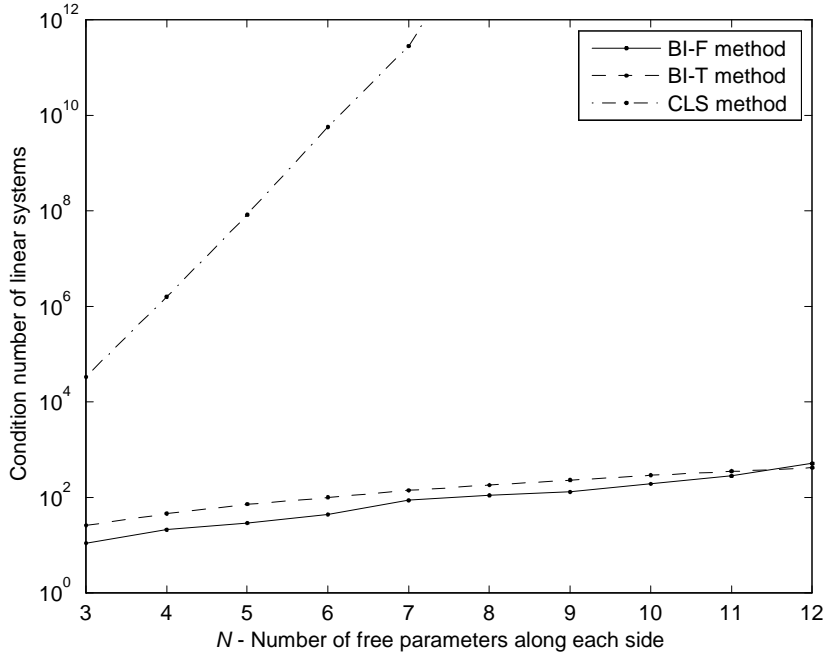


FIG. 5.2. *Test Case 1: Condition number of the linear systems to be solved vs. N - the number of free parameters used in the discretization along each side.*

| coefficients $\mu = 1-10$ | $\mu = 11-20$ | $\mu = 21-30$ |
|---------------------------|--------------------|--------------------|
| 1.127980401059388 | 0.000000921961930 | -0.000000000014456 |
| 0.169933866502253 | -0.000000155445876 | 0.000000000010590 |
| -0.023040973993480 | 0.000000108840774 | 0.000000000003894 |
| 0.003471196658216 | 0.000000037969831 | -0.000000000000718 |
| 0.000915157099087 | -0.000000006661925 | 0.000000000000531 |
| -0.000112803834456 | 0.000000004710615 | 0.000000000000197 |
| 0.000087716524487 | 0.000000001682649 | -0.000000000000037 |
| 0.000027760313669 | -0.000000000301797 | 0.000000000000027 |
| -0.000004416157802 | 0.000000000218392 | 0.000000000000010 |
| 0.000002753945681 | 0.000000000079333 | -0.000000000000002 |

TABLE 5.1
Corner function expansion coefficients for the CLS method on Test Problem 2

errors or data inaccuracies).

5.2. Test Case 2. The functions $g_\mu(r, \theta)$ defined in (2.8) satisfy the BCs on Sides 3 and 4. We base our CLS implementation on these functions ($\mu = 1, 2, 3, \dots$), collocating with the BCs along Sides 1 and 2. This gives (in less than 10 lines of Matlab code) the coefficient set shown in Table 5.1. These coefficient values are consistent with those presented in [3], but are probably more accurate since increasing the number of coefficients leaves the values shown in Table 5.1 invariant to all displayed decimal places (rather than causing higher decimal places to 'drift', leaving no reliable

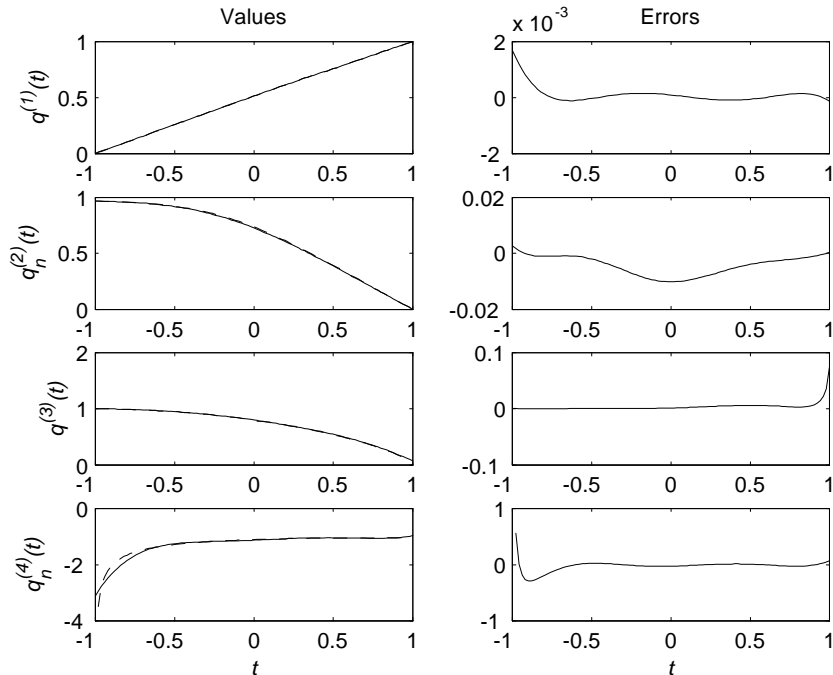


FIG. 5.3. *Test Case 2: Left column: Values computed by the BI-F method along the four sides (solid curves) vs. exact results (dashed curves), Right column: The errors along the sides.*

significant digits in [3] for coefficients past $\mu = 20$). The coefficients decay at a steady exponential rate that suggests a radius of convergence R_c of about $R_c = 2.4$. Thus the region of convergence extends across the full problem domain (for which no point is located further from the expansion corner than $\sqrt{2} \approx 1.4$). Such a large value for R_c should not be expected for more general BCs, but is a great convenience for this particular test problem since we therefore obtain a highly accurate reference solution to compare the numerical BI approaches against.

Since for this problem $q_n^{(4)}(t) \rightarrow -\infty$ when $t \rightarrow -1$ (recalling (2.8)), we cannot again display the max norm of the errors around the boundary. Instead, we display in Figure 5.3 the values computed by the BI-F method and their errors as functions of t along the four sides. In this computation, we have used a very coarse discretization: $N = 5$, i.e. only Legendre modes $P_0(t)$ to $P_4(t)$ along each side, and a total of 28 k -values (chosen within a radius $R = 15$ - as noted before not a particularly critical parameter setting). The errors are clearly dominated by the singularity at the 135° corner, corresponding to $t = 1$ for $q^{(3)}(t)$ and to $t = -1$ for $q_n^{(4)}(t)$. We next supplement the 20 expansion functions (the 5 Legendre polynomials along the 4 sides) with the most singular corner function $g_1(r, \theta) = r^{\frac{2}{3}} \sin(\frac{2}{3}\theta)$ (along Sides 3 and 4 only). For the same parameter settings, we now obtain the result shown in Figure 5.4. The corner error has dropped in size by several orders of magnitude, and it is no longer the dominant error. Also the errors are now smaller around all sides. In this calculation, the coefficient for the $g_1(r, \theta)$ -term becomes 1.1277 - a reasonable approximation to 1.1280. Increasing N (above 5) improves this approximation, and

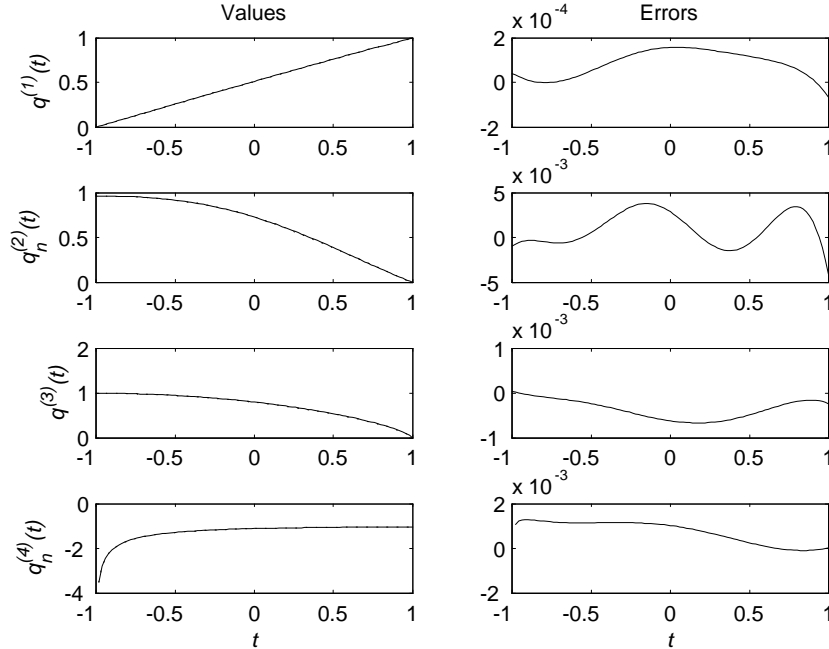


FIG. 5.4. *Test Case 2: Left column: Values along the four sides, computed by the BI-F method when including a single corner singularity function (solid curves) vs. exact results (dashed curves - invisible since covered by the solid curves), Right column: The errors along the sides.*

reduces the errors further along the sides. The inclusion of one (or more) corner singularity function leads again to integrals that can be evaluated in closed form, as is shown in Appendix C.

Since the primary goal of the present study is to verify the viability of the new BI-F formulation, we do not present test results here with the BI-T formulation for Test Problems 2 and 3. We only note that the same type of corner correction procedure is again available, although algebraically more complex. The counterparts to the integrals I_1 , I_2 , J_1 , J_2 in Appendix C can then be obtained from the closed form expression for $\int_{-1}^1 (1+t)^\alpha \log(t-z) dt$, which combines three ${}_2F_1$ hypergeometric functions.

5.3. Test Case 3. The CLS approach - immediate collocation along Sides 1 and 2 using the singularity functions $g_\mu(r, \theta)$ from (2.8) - gives for the leading coefficients the values shown in Table 5.2. These values (limited to the number of digits that can be believed to be reliable) are in excellent agreement with the result obtained in [2] (Table III), were they in turn were found to compare favorably against still other calculations in the literature. The coefficients decay to zero much slower than in Test Case 2. The present expansion's radius of convergence must satisfy $R_c \leq 1$ because of the singularity at the origin $(x, y) = (0, 0)$. In spite of the fact that the leading coefficients, as seen in Table 5.2, may give an appearance of decaying reasonably fast, the expansion cannot converge over the full domain. We nevertheless take it as the reference solution to compare against. The BI-F method (with $N = 5$, $R = 8$, no corner correction) produces the results shown in Figure 5.5. The largest discrepancy

| coeff. | $\mu = 1-5$ | $\mu = 6-10$ | $\mu = 11-15$ | $\mu = 16-20$ |
|--------|-------------|--------------|---------------|---------------|
| | 0.401931 | -0.004730 | -0.000395 | -0.000113 |
| | 0.093648 | -0.001545 | -0.000296 | -0.000092 |
| | -0.009383 | -0.001098 | -0.000219 | -0.000077 |
| | -0.029885 | -0.000719 | -0.000173 | -0.000065 |
| | -0.008359 | -0.000566 | -0.000138 | -0.000055 |

TABLE 5.2

Corner function expansion coefficients for the CLS method on Test Problem 3

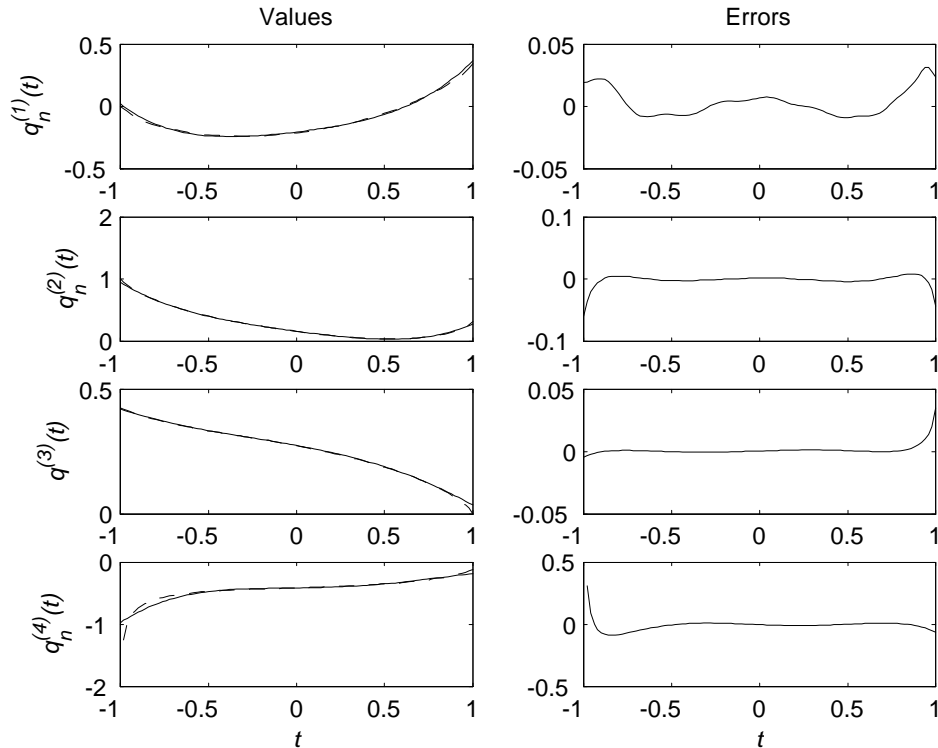


FIG. 5.5. Test Case 3: Left column: Values computed by the BI-F method along the four sides (solid curves) vs. the reference solution (dashed curves), Right column: The ‘errors’ - the differences to the reference solution along the sides, as obtained by the CLS method.

is clearly at the 135^0 corner. The wobbly fine structure of the ‘error’ along Side 1 corresponds to ‘noise’ in the badly determined reference solution and not to errors in the BI-F solution. We leave it as a future project to pursue corrections at all the four corners and to compare against more accurate reference solutions (which for example could be obtained via a conformal mapping approach).

6. Conclusions. Boundary integral (BI) methods are routinely used in a wide variety of applications, and the literature surrounding them is immense - including journals dedicated to the topic. It was therefore exciting when an altogether different BI formulation was proposed recently, based on the new ‘global equation’ approach arising from analytic function theory. This spectral space BI-F formulation is algebraically no more complex than earlier BI versions, and it leads to genuinely different

numerical implementation opportunities. We have shown here that it readily provides spectral accuracy and that it compares well against an also spectral implementation of the usual BI-T formulation. In particular, the new method gives rise to integrals that are either available in closed form or, when involving boundary data, have integrands that are just as smooth as the data. This is in distinct contrast to standard BI formulations, for which the required integrals can feature logarithmic singularities and sharp gradients.

The scope of this study has been limited to Laplace's equation on a single polygonal domain. Its goal has only been to highlight a novel opportunity that requires future studies before its place in the arsenal of numerical PDE methods can be properly assessed.

7. Acknowledgements. The work of Bengt Fornberg was supported by the NSF Grants DMS-0611681 and DMS-0914647. Natasha Flyer was supported by the NSF Grants ATM-0602100 and DMS-0934317. Numerous discussions with Professor Athanassios S. Fokas and with Christopher Ian Davis are gratefully acknowledged.

8. Appendix A. Selection of k -values - Halton nodes. The k -values we use should be well separated from each other, so that all the relations that are obtained by substituting them into (2.2), (2.3) will be relatively independent of each other. On the other hand, k -values of large magnitude will make the integrals strongly dominated by a very narrow range of z -values. Numerical experiments suggest it to be a good strategy to distribute the k -values somewhat randomly within a domain $|k| \leq R$, where R has to be appropriately chosen. Direct use of a random number generator is a bad strategy since, by the nature of randomness, dense clusters will occasionally form. Several options are available for creating scattered numbers that lack any apparent regularities, but which nevertheless will 'avoid' each other in a systematic manner. Halton nodes have this feature, and are particularly easy to generate. For example, the routine *haltonset* in Matlab's Statistics Toolbox or *haltonseq* from Matlab Central can be used to generate node sets in a d -dimensional unit cube. We use $d = 2$, and then ignore those falling outside the inscribed circle to the unit square. Translation and scaling will then provide good node sets satisfying $|k| \leq R$.

9. Appendix B. Closed form expressions for the integrals (3.10) and (3.11). The algorithm for evaluating the integrals $A_m(\alpha, \beta)$ and $B_m(\alpha, \beta)$ defined in (3.10) and (3.11) (for $\alpha \neq \pm 1$), starts by defining $z = \alpha + i\beta$, $L_1 = \log(-1 - \bar{z})$, $L_2 = \log(1 - \bar{z})$. One calculates

$$\begin{aligned} A_0(\alpha, \beta) &= -2 + (1 + z)L_1 - (-1 + z)L_2 \\ A_1(\alpha, \beta) &= -z + 0.5(-1 + z^2)(L_1 - L_2) \\ A_2(\alpha, \beta) &= 2/3 + z A_1(\alpha, \beta) \\ A_m(\alpha, \beta) &= ((2m - 1)z A_{m-1}(\alpha, \beta) - (m - 2) A_{m-2}(\alpha, \beta)) / (m + 1), \quad m = 3, 4, \dots \end{aligned} \tag{9.1}$$

and then discards the imaginary part of the obtained results. Similarly,

$$\begin{aligned} B_0(\alpha, \beta) &= i(L_1 - L_2) \\ B_1(\alpha, \beta) &= -2i + z B_0(\alpha, \beta) \\ B_m(\alpha, \beta) &= ((2m - 1)z B_{m-1}(\alpha, \beta) - (m - 1) B_{m-2}(\alpha, \beta)) / m, \quad m = 2, 3, \dots \end{aligned} \tag{9.2}$$

and again one discards the imaginary parts. The complex conjugates in the definitions of L_1 and L_2 ensure that, when using the standard convention for the branch cut of

the logarithm function, the result for $B_m(\alpha, 0)$ will agree with the limit $B_m(\alpha, \beta)$ for $\beta \searrow 0$.

The proofs for (9.1) and (9.2) are similar, so we give it only for the first case. The first three lines can be verified directly. Since

$$\operatorname{Re} \log(t - z) = \operatorname{Re} \log(t - \alpha - i\beta) = \log |t - \alpha - i\beta| = \log \sqrt{(\alpha - t)^2 + \beta^2},$$

the task is to show that the recursion holds for $A_m = \int_{-1}^1 P_m(t) \log(t - z) dt$, $m = 3, 4, \dots$. The standard three term recursion for Legendre polynomials can be written

$$mP_m(t) = (2m - 1)tP_{m-1}(t) - (m - 1)P_{m-2}(t).$$

Subtracting $(2m - 1)zP_{m-1}(t)$ from both sides, multiplying by $\log(t - z)$ and integrating in t from -1 to 1 gives

$$mA_m - (2m - 1)zA_{m-1} = \int_{-1}^1 (t - z) \log(t - z) (2m - 1)P_{m-1}(t) dt - (m - 1)A_{m-2}.$$

We next replace $(2m - 1)P_{m-1}(t)$ according to the identity $(2m - 1)P_{m-1}(t) = P'_m(t) - P'_{m-2}(t)$ and integrate by parts. The integral above then becomes

$$- \int_{-1}^1 (1 + \log(t - z))(P_m(t) - P_{m-2}(t)) dt = -A_m + A_{m-2} \quad (\text{when } m \geq 3),$$

and the recursion follows.

For given smooth functions $f(t)$, integrals of the types (3.6), (3.7) can be quickly and accurately evaluated by (i) evaluating $f(t)$ at *Chebyshev* node locations, in order to obtain its Chebyshev expansion coefficients by means of an FFT, (ii) converting these to Legendre expansion coefficients (for ex. by the *cheb2leg* routine from Matlab Central), and (iii) applying (9.1) and (9.2) to the resulting integrals.

10. Appendix C. Integrals arising when using corner singularity functions with the BI-F approach. To include the corner basis function

$$Q = r^{2/3} \sin \frac{2}{3}\theta$$

in the representations of the boundary functions along Sides 3 and 4, the key relations that need to be considered are:

Side 3:

$$\begin{aligned} z &= 1 + 2i - \frac{1}{2}(t + 1)(1 + i), & \frac{dz}{dt} &= -\frac{1}{2}(1 + i), & \frac{ds}{dt} &= \frac{1}{\sqrt{2}} \\ Q &= \frac{1}{2^{1/3}}(1 - t)^{2/3}, & Q_n &= 0 \\ I_1 &= \int_{-1}^1 (e^{-ikz} k \frac{dz}{dt} Q) dt &= (-1 - i)2^{1/3} e^k k H(\frac{5}{3}, (-1 + i)k) \\ I_2 &= \int_{-1}^1 (e^{-ik\bar{z}} k \frac{d\bar{z}}{dt} Q) dt &= (-1 + i)2^{1/3} e^k k H(\frac{5}{3}, (-1 - i)k) \end{aligned}$$

Side 4:

$$\begin{aligned} z &= i - \frac{i}{2}(t + 1), & \frac{dz}{dt} &= -\frac{i}{2}, & \frac{ds}{dt} &= \frac{1}{2} \\ Q &= 0, & Q_n &= -\frac{2^{4/3}}{3}(1 + t)^{-1/3} \\ J_1 &= \int_{-1}^1 (e^{-ikz} \frac{ds}{dt} Q_n) dt &= -\frac{2}{3} e^k H(\frac{2}{3}, k) \\ J_2 &= \int_{-1}^1 (e^{-ik\bar{z}} \frac{d\bar{s}}{dt} Q_n) dt &= J_1 \end{aligned}$$

Here, $H(a, z) = z^{-a} \int_0^z t^{a-1} e^{-t} dt$. Although the integral itself is well known as the incomplete gamma function, it is better to work with $H(a, z)$ because this is an entire function (and not a multivalued function with a singularity at the origin). From a numerical perspective, the continued fraction expansion for $H(a, z)$ is particularly convenient to use:

$$H(a, z) = e^{-z} \cdot \frac{1}{a - \frac{az}{a+1 + \frac{z}{a+2 - \frac{(a+1)z}{a+3 + \frac{2z}{a+4 - \frac{(a+2)z}{a+5 + \frac{3z}{a+6 - \dots}}}}}}}$$

For effective numerical evaluation of such expansions (e.g. the algorithms by Steed and Lentz), see for ex. [17]. This same approach - reformulating boundary integrals to H -functions - will apply to every one of the corner singularity functions given by (2.8).

REFERENCES

- [1] Driscoll, T.A. and Trefethen, L.N., Schwarz-Christoffel mapping, Cambridge University Press (2002).
- [2] Elliotis, M., Georgiou, G. and Xenophontos, C., The solution of Laplacian problems over L-shaped domains with a singular function boundary integral method, *Comm. Numer. Meth. Eng.* 18 (2002), 213-222.
- [3] Elliotis, M., Georgiou, G. and Xenophontos, C., Solving Laplacian problems with boundary singularities: a comparison of a singular function boundary integral method with the p/hp version of the finite element method, *Appl. Math. Comp.* 169 (2005), 485-499.
- [4] Flyer, N. and Fokas, A.S., A hybrid analytical-numerical method for solving evolution PDEs. I. The half-line. *Proc. R. Soc. Lond. A.* 464 (2008), 1823-1849.
- [5] Flyer, N. and Fornberg, B., On the nature of initial-boundary value solutions for dispersive equations, *SIAM J. Appl. Math.* 64 (2003), 546-564.
- [6] Fokas, A.S., A unified transform method for solving linear and certain nonlinear PDEs, *Proc. R. Soc. A* 453 (1997), 1411-1443.
- [7] Fokas, A.S., Two dimensional linear PDEs in a convex polygon, *Proc. R. Soc. A* 457 (2001), 371-393.
- [8] Fokas, A.S., A new transform method for evolution PDEs, *IMA J. Appl. Math.* 67 (2002), 559-590.
- [9] Fokas, A.S. and Pelloni, B., A transform method for evolution PDEs on finite interval, *IMA J. Appl. Math.* 70 (2005) 564-587.
- [10] Fokas, A.S., A Unified Approach to Boundary Value Problems, SIAM, Philadelphia (2008).
- [11] Fokas, A.S., Flyer, N., Smitheman, S.A. and Spence, E.A., A semi-analytical numerical method for solving evolution and elliptic partial differential equations, *J. Comp. Appl. Math.* 227 (2009), 59-74.
- [12] Fulton, S., Fokas, A.S. and Xenophontos, C., An analytical method for linear elliptic PDEs and its numerical implementation, *J. Comput. Appl. Math.* 167 (2004), 465-483.
- [13] Igarashi, H. and Honma, T., A boundary element method for potential fields with corner singularities, *Appl. Math. Model.* 20 (1996), 847-852.
- [14] Georgiou, G.C., Olson, L. and Smyrlis, Y.S., A singular function boundary integral method for the Laplace equation, *Comm. Num. Meth. Eng.* 12 (1996), 127-134.
- [15] Li, Z.C. and Lu, T.T., Singularities and treatments of elliptic boundary value problems, *Math. Comp. Modelling*, 31 (2000), 97-145.
- [16] Pozrikidis, A Practical Guide to Boundary Element Methods with the Software Library BEM-LIB, Chapman & Hall/CRC, Boca Raton, FL (2002).
- [17] Press, W.H., Flannery, B.P., Teukolsky, S.A. and Vetterling, W.T., Numerical Recipes in C: The Art of Scientific Computing, Cambridge University Press (1992).

- [18] Sifalakis, A.G., Fokas, A.S., Fulton, S.R. and Saridakis, Y.G., The generalized Dirichlet-Neumann map for linear elliptic PDEs and its numerical implementation, *J. Comput. Appl. Math.*, 219 (2008), 9-34.